Breaking the limitations of local impedance noise control: passivity and scattering performances of the Advection Boundary Law

Emanuele de Bono, Manuel Collet, Morvan Ouisse

Breaking the limitations of local impedance noise control: passivity and scattering performances of the Advection Boundary Law

Emanuele De Bono [1], **Manuel Collet** [1]
[1] Ecole Centrale de Lyon, CNRS, ENTPE, LTDS, UMR5513, 69130 Ecully, France
emanuele.de-bono@ec-lyon.fr

Morvan Ouisse [2]
[2] SUPMICROTECH, Université de Franche-Comté, CNRS, institut FEMTO-ST, F-25000 Besançon, France.

May 29, 2024

Abstract

In the aim of attenuating noise transmission through air-ducts, research is prompted for overcoming the limitations of classical acoustic liners, especially in the aero-engines applications. The new generation of Ultra-High-By-Pass-Ratio (UHBR) turbofans while considerably reducing fuel consumption, increases noise pollution especially at lower frequencies because of their larger diameter, lower number of blades and rotational speed. Moreover, they present a shorter nacelle, leaving less available space for acoustic treatments. In case of simplified one-dimensional propagation, integral constraints exist which analytically define the limits of the scattering performances of reciprocal systems, such they are the local impedance liners, for a fixed length of the acoustic treatment along the duct. In this contribution, we analyse a special boundary condition breaking the reciprocity principle, and overcoming the limitations of locally reacting liners. We call it Advection Boundary Law as it introduces a convection on the boundary, responsible of non-reciprocal behaviour at grazing incidence, and of the enhancement of transmission loss with respect to pure locally-reacting resonators. Performances and passivity of such boundary law are numerically analysed first in grazing-incidence problems. The grazing-incidence problem is experimentally studied in a plane-wave acoustic waveguide lined by

electroacoustic resonators which can be programmed to reproduce such advection boundary law.

1 INTRODUCTION

The acoustic problem of interest here, is the noise transmission mitigation in an open duct, by treatment of the parietal walls with a so-called liner. Examples of industrial fields where this problem is particularly felt are the Heating and Ventilation Air-Conditioning Systems (HVAC) and the turbofan aircraft engines. The new generation of Ultra-High-By-Pass-Ratio (UHBR) turbofans, in order to comply with the significant restrictions on fuel consumptions and pollutant emissions, present larger diameter, lower number of blades and rotational speed and a shorter nacelle. These characteristics conflict with the equally restrictive regulations on noise pollution, as the noise signature is shifted toward lower frequencies, which are much more challenging to be mitigated. The acoustic liner technology applied nowadays for noise transmission attenuation at the inlet and outlet portions of turbofan engines is the so-called Single or Multi-Degree-of-Freedom liner, whose working principle relates to the quarter-wavelength resonance, and demands larger thicknesses to target lower frequencies. They are made of a closed honeycomb structure and a perforated plate which is used to provide the dissipative effect, to add mass in order to decrease the resonance frequency, and also to maintain the aerodynamic flow as smooth as possible on the internal wall of the nacelle. As the honeycomb structure is impervious, propagation is prevented transversely to the wall, therefore it can be considered as *locally reacting* as long as the incident field wavelength is much larger than the size of the honeycomb cells [18].
The Electroacoustic Resonator (ERs) is made of a drivable speaker collocated with one or more microphone. Its impedance can be controlled by a pressure-based current-driven architecture [24]. Despite the physiological time delay of the digital control, which can affect the passivity margins at high frequencies [9], such ER strategy has demonstrated its efficiency for both room-modal equalization [25] and sound transmission mitigation in waveguides [5, 1, 4, 3, 2]. The model-inversion algorithm has also been extended to contemplate nonlinear target dynamics at low excitation levels [10, 8, 19, 20]. In [6], for the first time, a programmable liner involving the spatial derivative was realised by distributed electroacoustic devices. It was the first form of the Advection Boundary Law (ABL), then implemented on ER arrays lining an acoustic waveguide in [17, 13, 12], where it demonstrated non-reciprocal

sound propagation. Non-reciprocal propagation is a highly desirable feature for many physical domains and applications [14]. Nevertheless, because of its spatial non-locality, the conceptual categories defining the passivity of a surface impedance (see [23]) do not apply to the ABL. In this contribution, we provide an analysis of the passivity limits and performances of the ABL, excited by plane waves and in absence of airflow. In Section 2, we provide the duct-mode analysis in a 2D waveguide, which allows to define the passivity limits of the ABL. In Section 3, we present the scattering simulations in a 2D duct lined by our ABL. Finally, in Section 4, the potentialities of the ABL are validated in an experimental test-rig, in terms of enhanced isolation and non-reciprocal propagation. The overall achievements and next steps are finally discussed in Section 5.

2 Duct modes analysis in 2D waveguide

The ABL can be written as:

$$Z_{Loc}(\partial_t) * \partial_t v_n = \partial_t p + U_b \partial_x p \quad \text{on } \partial\Omega, \tag{1}$$

where $Z_{Loc}(\partial_t)$ is the differential operator in time domain corresponding to a local complex impedance, $*$ is the convolution operation, v_n is the velocity normal to the boundary $\partial\Omega$, p is the acoustic pressure, and U_b is the advection speed. We define $M_b = U_b/c_0$.

Let us investigate the passivity and attenuation performances into an acoustic waveguide starting from the duct mode analysis. Duct modes are fundamental to understand the propagation characteristics in a waveguide. We consider a 2D duct of section width $h = 0.05$ m, with both upper and lower walls lined by the ABL. According to the assumption of duct mode eigen-solution $\bar{p}_m(t, \omega, x, y) = A_m \psi_m(y, \omega) e^{\mathrm{j}\omega t - \mathrm{j}k_{x,m}(\omega)x}$, the duct mode analysis consists in computing the duct-mode eigenvalues ($k_{x,m}$) and eigenvectors (ψ_m), while A_m can be normalized at will. The local impedance, and hence the local normalized mobility $\eta_{Loc} = 1/\zeta_{Loc} = \rho_0 c_0 / Z_{Loc}$, is considered as purely real.

In Fig.s 2 and 3 the first eight solutions in terms of wavenumbers and corresponding duct modes respectively, are plotted. The frequency span is limited between 150 and 3000 Hz to focus on the same frequency range as the experimental results. Moreover, one can notice that mode 1^+ is attenuated ($\mathrm{Im}\{k_{x,1^+}\} < 0$), while mode 1^- is a plane wave ($\psi_1^- = 1$, $k_{x,1^-} = -k_0$). This demonstrates *the breaking of the reciprocity principle* [15] in the plane wave

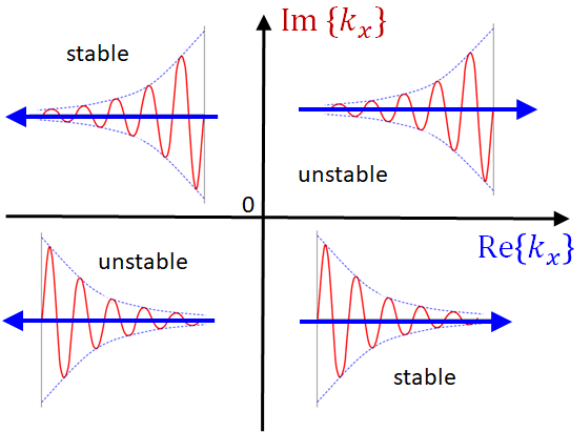

Figure 1. Stability regions of duct-modes in the (Re{k_x},Im{k_x})-plane.

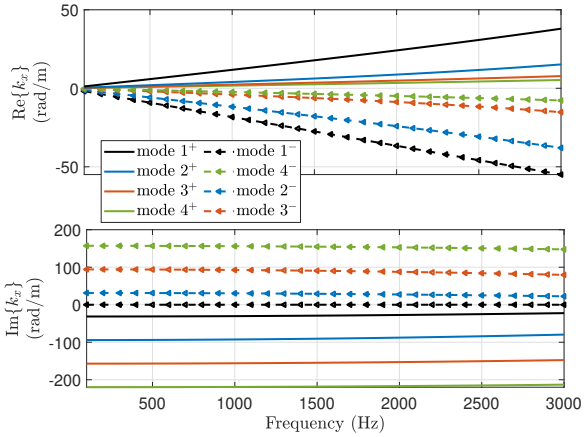

Figure 2. Dispersion plots for the wavenumbers relative to the first four duct modes propagating in both senses, in case of boundary advection law with $\eta_{Loc} = 1$ and $M_b = -1$.

regime, as it will be clearer in the following.

In this contribution we focus just on the first forward and backward propagating mode (1^+ and 1^-), as we are interested in the isolation performances in the plane wave regime of a rigid duct. Indeed, the first modes are also the least attenuated ones, therefore mostly ruling the noise transmission when the liner is applied in a segment of a rigid duct [21, 7]. Fig. 4 shows the frequency plots of Re$\{k_{x,m}\}$ and Im$\{k_{x,m}\}$, for modes $m = 1^+$ and $m = 1^-$.

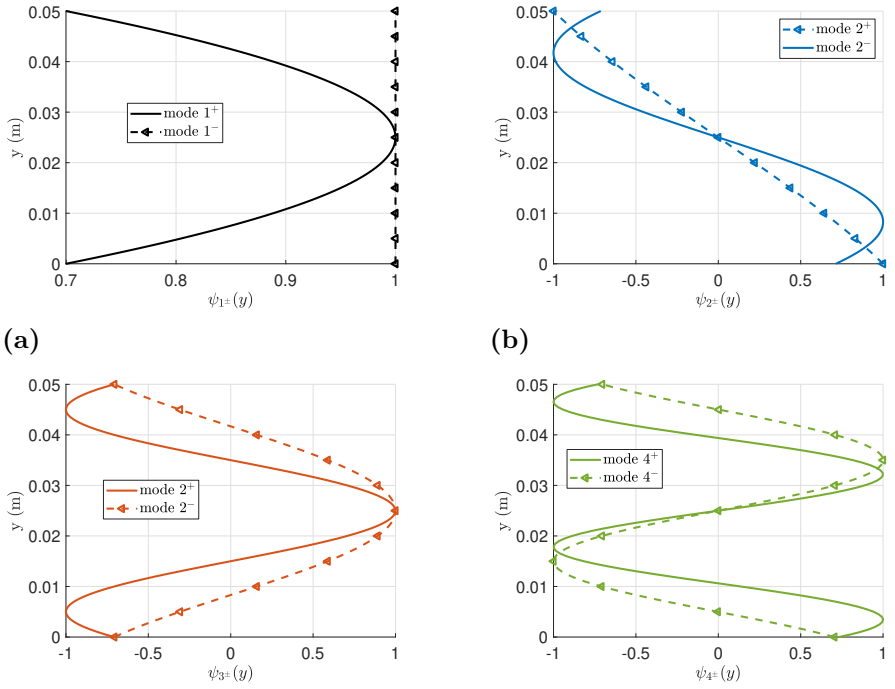

(a) **(b)**

(c) **(d)**

Figure 3. First four duct mode-shapes $\psi_m(y)$, propagating toward positive and negative x direction, normalized with respect to the maximum value, for ABL treated boundaries with $\eta_{Loc} = 1$ and $M_b = -1$, at 500 Hz.

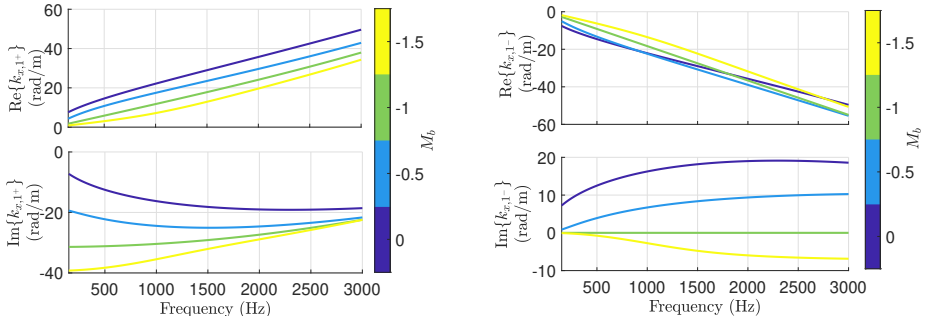

(a) **(b)**

Figure 4. Spectra of $\mathrm{Re}\{k_{x,m}\}$ and $\mathrm{Im}\{k_{x,m}\}$, with $\eta_{Loc} = 1$ and varying $M_b < 0$, for mode $m = 1^+$ **(a)** and $m = 1^-$ **(b)**.

Looking at Fig. 4b, we observe that for $M_b = -1$, mode 1^- becomes a plane wave, while for $M_b < -1$ we have non-stable duct mode propagation. Looking at Fig. 4a, notice the monotonic increase of $\mathrm{Im}\{k_{x,1^+}\}$ with $|M_b|$, confirming the higher attenuation performances achievable thanks to the ABL with $M_b < 0$ with respect to local impedance operators ($M_b = 0$).

3 Scattering simulations in 2D waveguide

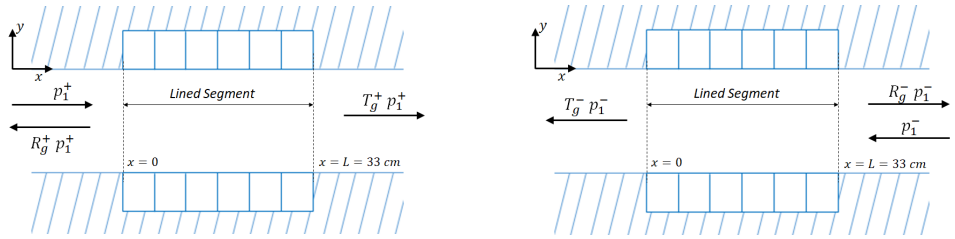

(a) **(b)**

Figure 5. Lining segment and scattering coefficients definition in a 2D waveguide lined on both sides.

In this section the ABL is analysed in terms of scattering performances in the plane wave regime. The liner is considered to extend for an axial length $L = 0.3$ m in a 2D acoustic waveguide of cross-section height $h = 0.05$ m, without flow. Such dimensions correspond to the experimental setup that will be presented in Section 4. The scattering problem is illustrated in Fig. 5, where the reflection R_g and transmission T_g coefficients are defined for incident field directed toward either $+x$ or $-x$. The subscript g is employed to indicate the *grazing* incidence. The ABL is applied continuously on the boundary of the waveguide in the lined segment. The scattering matrix is defined in Eq. (2) for the plane wave regime of a hard-walled duct.

$$\begin{bmatrix} p_2^+ \\ p_1^- \end{bmatrix} = \begin{bmatrix} T_g^+ & R_g^- \\ R_g^+ & T_g^- \end{bmatrix} \begin{bmatrix} p_1^+ \\ p_2^- \end{bmatrix}. \tag{2}$$

The superscript signs $+$ or $-$ in Eq. (2), indicate the direction of propagation of the incident plane wave (toward either $+x$ or $-x$). The results in terms of scattering matrix coefficients, have been obtained by FE simulations in Comsol. As in the duct mode analysis, the FE mesh has been built sufficiently fine to fully resolve both longitudinal and transversal pressure field up to $f_{max} = 3$ kHz. The scattering coefficients $T_g^{\pm}$ and $R_g^{\pm}$ are computed, by exciting first the left and then the right termination. In

the scattering problem, high noise isolation toward $+x$ ($-x$) corresponds to low values of T_g^+ (T_g^-). The acoustical passivity, in the plane wave regime, corresponds to positive values of both α_g^+ and α_g^-.
As in the duct mode analysis, we consider the case of purely real Z_{Loc} in the ABL. The scattering performances are presented in terms of power scattering coefficients for both positive and negative propagation. The power scattering coefficients are defined from the power balance [16] which, in case of plane waves, reduces to:

$$1 = \alpha_g^{\pm} + |T_g^{\pm}|^2 + |R_g^{\pm}|^2, \tag{3}$$

where R_g and α_g are the reflection and absorption coefficients in grazing incidence, respectively. From $|T_g^{\pm}|^2$, it is possible to compute the Transmission Loss $(TL_g^{\pm})_{Liner} = 10\log_{10}(1/|T_g^{\pm}|^2)$, and the Insertion Loss $IL_g^{\pm} = (TL_g^{\pm})_{Liner} - (TL^{\pm})_{Rigid}$. As $(TL^{\pm})_{Rigid} = 0$ in simulations, $IL^{\pm} = (TL_g^{\pm})_{Liner}$.

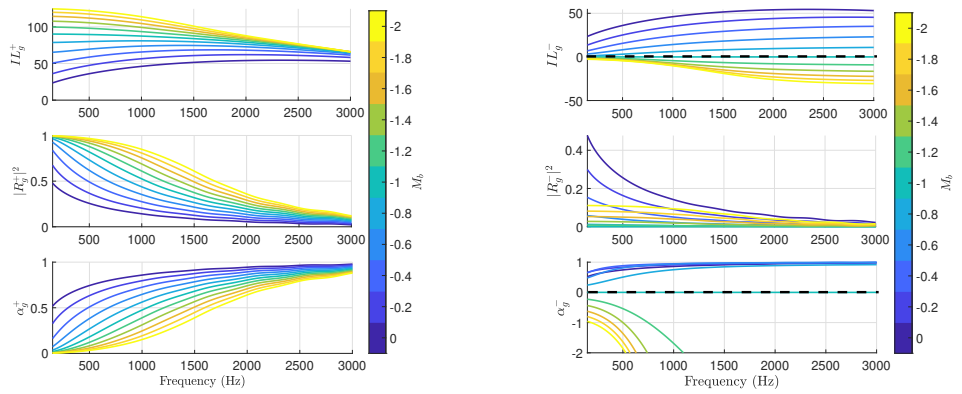

(a) **(b)**

Figure 6. Scattering coefficients in a 2D waveguide of cross section width $h = 0.05$ m with lined segment of length $L = 0.3$ m, lined on both sides by the boundary advection law with $\zeta_{Loc} = 1$, and varying M_b.

Fig. 6a shows the power scattering coefficients in case of $\zeta_{Loc} = 1$, for M_b continuously varying from 0 to -2. Coherently with the duct mode 1^+ solution reported in Section 2, increasing the absolute value of $M_b < 0$, brings about an increase in the IL_g^+, especially at low frequencies. Observe that such increase of IL_g^+ is accompanied by a significant increment of the back-reflection and, less intuitively, by a reduction of absorption. This means that, in such configuration of waveguide with both upper and lower sides

lined by the ABL, excited by plane waves propagating against the boundary advection speed, most energy is reflected back rather being absorbed. In case of negative propagation, i.e. plane waves propagating concordant with M_b, perfect transmission is assured for $M_b = -1$, while for $M_b < -1$, the loss of passivity ($\alpha_g^{-1} < 0$) of the ABL manifests itself by $|T_g^-| > 1$ in agreement with the change of sign of $\mathrm{Im}\{k_{x,1^+}\}$ showed in Fig. 4b. The passivity limits are highlighted by dashed black line in Fig. 6. These results are totally coherent with the results of Section 2 both in terms of attenuation performances and passivity. Moreover, perfect non-reciprocal propagation is achieved for $M_b = -1$, as $IL_g^- = 0$, while IL_g^+ is very high. This, also, is in agreement with the dispersion solutions of Section 2.

4 Experimental results

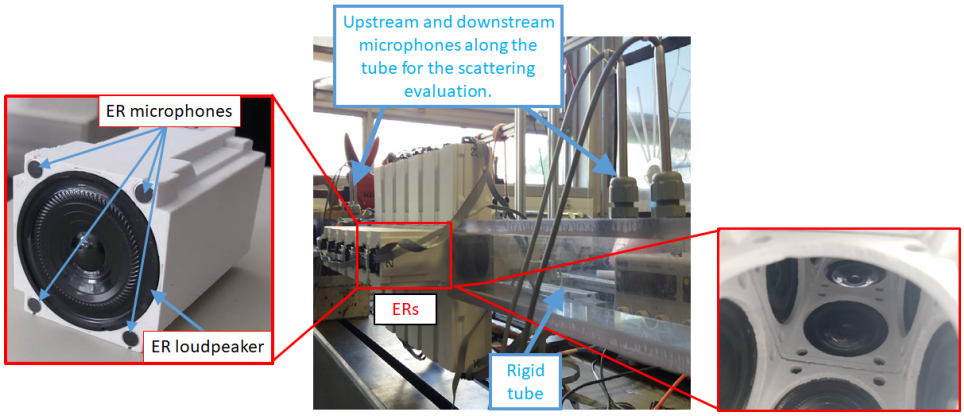

Figure 7. ER prototype (left); waveguide (middle) for the scattering evaluation, with internal view of the lined segment (right).

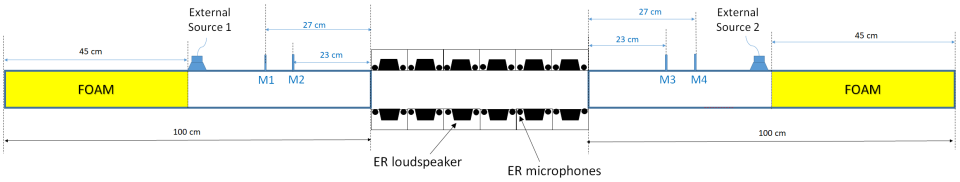

Figure 8. Sketch of the test-bench.

In this section, the advection control law is experimentally tested on an array of 24 ER prototypes lining a squared cross-section duct of about 0.05

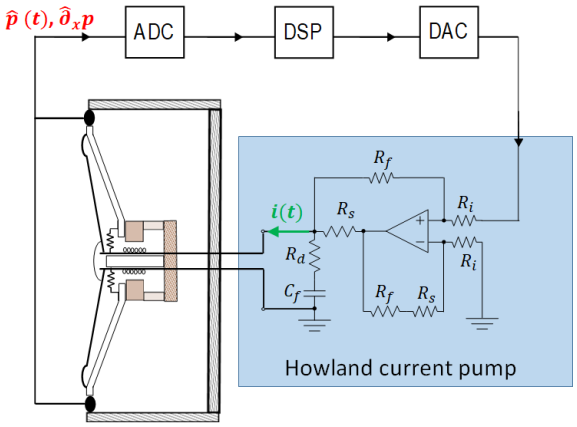

Figure 9. Sketch of the ER architecture.

m side, as illustrated in the photos of Fig. 7 and in the sketch of Fig. 8. The ERs are placed 6 per each side of the duct, as showed in Fig. 7. Each ER has a surface area of about $0.05 \times 0.05\ m^2$, for a total lined segment length of about 0.3 m in the duct. Both ends of the tube are filled with 45 cm of foam to reproduce quasi-anechoic conditions at the input and output of the waveguide. An external acoustic source is placed flush with the duct surface on both sides of the waveguide, just ahead of the foam terminations, sufficiently far from the lined segment and from microphone locations. The external sources are excited with a sine-sweep signal from 150 Hz (lower limit of the source-loudspeakers) to 3 kHz (to stay below the cut-on frequency of the higher rigid duct modes).

Each ER is controlled autonomously, and the control architecture is illustrated in Fig. 9: the signals $\hat{p}$ and $\hat{\partial}_x p$ on the speaker diaphragm, after being digitally converted by the Analogue-Digital-Converter (ADC), are fed into a *programmable* digital signal processor (DSP) where the output of the control is computed at each time step. The Howland current pump [22] allows to enforce the electrical current i in the speaker coil independently of the voltage at the loudspeaker terminals. It consists of an operational amplifier, two input resistors R_i, two feedback resistors R_f, and a current sense resistor R_s. The resistance R_d and capacitance C_f constitutes the compensation circuit to ensure stability with the grounded load [26]. More details can be found in [9]. All ERs and control interfaces have been produced in the Department of Applied Mechanics at FEMTO-st Institute. The control law is given in [11].

The four scattering coefficients have been estimated according to the two-source method [21]. Fig. 10 shows the experimental scattering coefficients

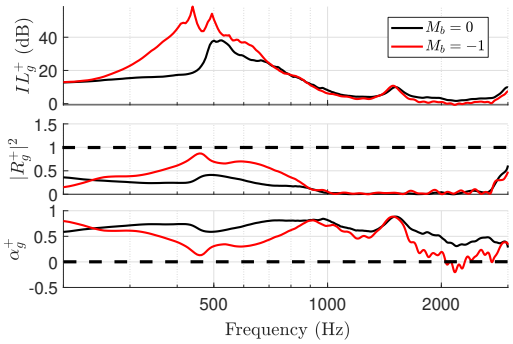

Figure 10. Experimental scattering performances for incident field propagating toward $+x$, achieved by the ABL with varying M_b (**a**), or varying R_d. The default parameters are set to $\mu_M = \mu_K = 0.5$, $R_d = \rho_0 c_0$ and $M_b = -1$.

for incident field toward $+x$, with varying M_b and R_d respectively. Fig. 10 confirms the higher isolation achieved by the ABL (with $M_b = -1$) with respect to the local impedance control ($M_b = 0$). Observe, in Fig. 10, the reduction of passivity from 1.8 kHz and above with higher $|M_b|$. This is due to a combined effect of time delay [9] and the first order approximation of $\hat{\partial}_x p$, which is clearly amplified for higher values of $|M_b|$.

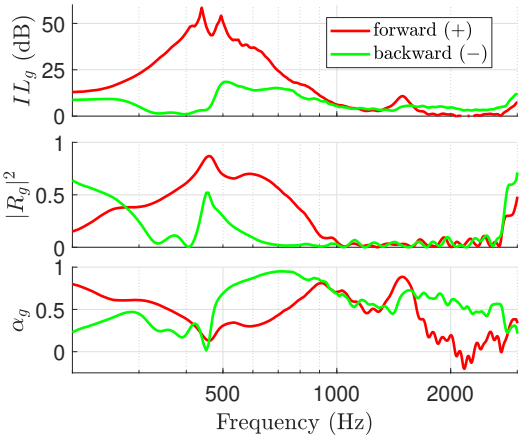

Figure 11. Scattering performances relative to external incident field propagating toward $+x$ ("forward", in solid red) compared to the ones relative to "backward" incident field (in solid green), in case of ABL with $M_b = -1$.

The broadband non-reciprocal character of the advective BC is evident by looking at Fig. 11, where the "forward" scattering coefficients (corresponding

to the first column of the scattering matrix of Eq. (2)), are plotted along with the "backward" scattering coefficients (corresponding to the second column of the scattering matrix of Eq. (2)), in case of $M_b = -1$. Observe that, in the backward direction, we do not have perfect transmission, due to the limitations of the control law [9]. Nevertheless, IL_g^- never overcomes 18 dB, while for forward propagation IL_g^+ is significantly higher than 25 dB from 300 to 700 Hz, and higher than 50 dB close to resonance. Notice that such non-reciprocal propagation is achieved in the bandwidth of ζ_{Loc}, while in [17] it was accomplished only above resonance. This is due to the different definitions of the correctors in the control law, which are here targeting the frequency range around ζ_{Loc} resonance, allowing to significantly enhance both isolation and non-reciprocal performances in the target bandwidth.

5 Conclusions

In this contribution, we have provided a discussion of the Advection Boundary Law, which is composed of a local impedance component and a convective term. We discuss the duct-mode solutions in a 2D waveguide without flow in Section 2 in case of purely real local impedance term. The 2D duct-mode analysis is followed by the resolution of the 2D scattering problem. The correlation between the two studies is evident, in terms of passivity, attenuation levels and non-reciprocal propagation.

An array of programmable Electroacoustic Resonators lining an acoustic waveguide allows to implement the Advection Boundary Law in real life. The measurements validate the Advection Boundary Law accomplishments in terms of enhanced isolation, passivity and non-reciprocal sound propagation, despite the physiological limitations of digital control algorithms.

Because of its non-natural and non-local character, special attention must be given when implementing the Advection Boundary Law. In this paper, we have provided some numerical tools to guide the control users when implementing such special boundary control, in order to maximize its isolation performances, avoid non-passive behaviours, and/or achieve the desired non-reciprocal propagation. This first study has analysed the Advection Boundary Law in the plane-wave regime and in absence of mean flow. Such work has put the necessary bases for the Advection Boundary Law to tackle more complex guided propagation problems, including airflow convection and multi-modal propagation.

References

[1] K Billon, E De Bono, M Perez, E Salze, G Matten, M Gillet, M Ouisse, M Volery, H Lissek, J Mardjono, and Others. In flow acoustic characterisation of a 2D active liner with local and non local strategies. *Applied Acoustics*, 191:108655, 2022.

[2] K Billon, M Gillet, E Salze, Maxime Volery, E De Bono, M Ouisse, Hervé Lissek, Manuel Collet, and J Mardjono. Smart acoustic lining for UHBR technologies engine: from the design of an electroacoustic metasurface to experimental characterization under flow. In *Active and Passive Smart Structures and Integrated Systems XVII*, volume 12483, pages 390–396. SPIE, 2023.

[3] Kevin Billon, Manuel Collet, Edouard Salze, Martin Gillet, Morvan Ouisse, Maxime Volery, Hervé Lissek, and Jacky Mardjono. 2D active liner experimental results in acoustic flow duct facility. In *Smart Materials, Adaptive Structures and Intelligent Systems*, volume 86274, page V001T03A001. American Society of Mechanical Engineers, 2022.

[4] Kevin Billon, E De Bono, M Perez, E Salze, G Matten, M Gillet, M Ouisse, M Volery, H Lissek, J Mardjono, and Others. Experimental assessment of an active (acoustic) liner prototype in an acoustic flow duct facility. In *Health Monitoring of Structural and Biological Systems XV*, volume 11593, page 115932L. International Society for Optics and Photonics, 2021.

[5] R. Boulandet, H. Lissek, S. Karkar, M. Collet, G. Matten, M. Ouisse, and M. Versaevel. Duct modes damping through an adjustable electroacoustic liner under grazing incidence. *Journal of Sound and Vibration*, 426:19–33, jul 2018.

[6] Manuel Collet, Petr David, and Marc Berthillier. Active acoustical impedance using distributed electrodynamical transducers. *The Journal of the Acoustical Society of America*, 125(2):882–894, 2009.

[7] L Cremer. Theory regarding the attenuation of sound transmitted by air in a rectangular duct with an absorbing wall, and the maximum attenuation constant produced during this process. *Acustica*, 3(1):249, 1953.

[8] Camila Elizabeth da Silveira Zanin, Aurélie Labetoulle, Emanuele De Bono, Emmanuel Gourdon, Manuel Collet, and Alireza Ture Savadkoohi.

Experimental evidences of nonlinear programmable electroacoustic loudspeaker. *Building Acoustics*, 30(3):249–263, 2023.

[9] E De Bono, M Collet, G Matten, S Karkar, H Lissek, M Ouisse, K Billon, T Laurence, and M Volery. Effect of time delay on the impedance control of a pressure-based, current-driven Electroacoustic Absorber. *Journal of Sound and Vibration*, page 117201, 2022.

[10] E. De Bono, M. Morell, M. Collet, E. Gourdon, A. Ture Savadkoohi, M. Ouisse, and C.H. Lamarque. Model-inversion control to enforce tunable Duffing-like acoustical response on an Electroacoustic resonator at low excitation levels. *Journal of Sound and Vibration*, 570:118070, feb 2024.

[11] Emanuele De Bono. *Electro-active boundary control for noise mitigation: local and advective strategies*. PhD thesis, Université de Lyon, 2021.

[12] Emanuele de Bono, Manuel Collet, Edouard Salze, Morvan Ouisse, Martin Gillet, Hervé Lissek, Jacky Mardjono, Kévin Billon, and Maxime Volery. Advection boundary law for sound transmission attenuation of place and spinning guided modes. In *Forum Acusticum*, 2023.

[13] Emanuele De Bono, Morvan Ouisse, Manuel Collet, Edouard Salze, and Jacky Mardjono. A nonlocal boundary control, from plane waves to spinning modes control. In *Active and Passive Smart Structures and Integrated Systems XVII*, volume 12483, page 124831B. SPIE, 2023.

[14] Romain Fleury, Dimitrios Sounas, Michael R Haberman, and Andrea Alu. Nonreciprocal acoustics. *Acoustics Today*, 11(ARTICLE):14–21, 2015.

[15] Romain Fleury, Dimitrios L Sounas, and Andrea Alù. Subwavelength ultrasonic circulator based on spatiotemporal modulation. *Physical Review B*, 91(17):174306, may 2015.

[16] Uno Ingard. *Noise reduction analysis*. Jones & Bartlett Publishers, 2009.

[17] Sami Karkar, Emanuele De Bono, Manuel Collet, Gaël Matten, Morvan Ouisse, and Etienne Rivet. Broadband Nonreciprocal Acoustic Propagation Using Programmable Boundary Conditions: From Analytical Modeling to Experimental Implementation. *Physical Review Applied*, 12(5):054033, nov 2019.

[18] XuQiang Ma and ZhengTao Su. Development of acoustic liner in aero engine: a review. *Science China Technological Sciences*, pages 1–14, 2020.

[19] Maxime Morell, Manuel Collet, Emmanuel Gourdon, and Alireza Ture Savadkoohi. Control of an acoustic mode by a digitally created Nonlinear Electroacoustic Absorber at low excitation levels: Analytical and Experimental results. In *Surveillance, Vibrations, Shock and Noise*, 2023.

[20] Maxime Morell, Emmanuel Gourdon, Manuel Collet, Alireza Ture Savadkoohi, and Emanuele De Bono. NONLINEAR DIGITALLY CREATED ELECTROACOUSTIC ABSORBER DESIGNED FOR ACOUSTIC ENERGY PUMPING. 2023.

[21] M L Munjal and A G Doige. Theory of a two source-location method for direct experimental evaluation of the four-pole parameters of an aeroacoustic element. *Journal of Sound and Vibration*, 141(2):323–333, 1990.

[22] Robert A Pease. A Comprehensive Study of the Howland Current Pump A Comprehensive Study of the Howland Current Pump Applications for the Howland Current Pump AN-1515. *Most*, 29:12, 2008.

[23] Sjoerd W Rienstra. Fundamentals of duct acoustics. *Von Karman Institute Lecture Notes*, 2015.

[24] Etienne Rivet, Sami Karkar, and Herve Lissek. Broadband Low-Frequency Electroacoustic Absorbers Through Hybrid Sensor-/Shunt-Based Impedance Control. *IEEE Transactions on Control Systems Technology*, 25(1):63–72, jan 2017.

[25] Etienne Thierry Jean-Luc Rivet. *Room Modal Equalisation with Electroacoustic Absorbers*. PhD thesis, EPFL, 2016.

[26] Jerry Steele and Tim Green. Tame those versatile current source circuits. *Electronic Design*, 61, 1992.